PERSPECTIVE

Correlating polymer structure, dynamics, and function with atomic force microscopy

Julia G. Murphy [ID] | **Jonathan G. Raybin** [ID] | **Steven J. Sibener** [ID]

The James Franck Institute and Department of Chemistry, The University of Chicago, Chicago, Illinois, USA

Correspondence
S. J. Sibener, The James Franck Institute and Department of Chemistry, The University of Chicago, 929 E. 57 Street, Chicago, IL 60637, USA.
Email: s-sibener@uchicago.edu

Present address
Jonathan G. Raybin, Department of Chemistry, University of California Berkeley, Berkeley, California, USA

Funding information
NSF Materials Research Science and Engineering Center (MRSEC), Grant/Award Number: NSF-DMR-2011854; U.S. Department of Commerce, National Institute of Standards and Technology as part of the Center for Hierarchical Materials Design (CHiMaD), Grant/Award Number: 70NANB19H005; Advanced Materials for Energy-Water Systems (AMEWS) Center, an Energy Frontier Research Center funded by the US Department of Energy, Office of Science, Basic Energy Sciences

Abstract

Since its development, atomic force microscopy (AFM) has become an indispensable tool for investigating fundamental and technological applications of polymer materials. The versatility of AFM imaging modes and operating conditions allows for nanoscale characterization of a range of dynamic processes, such as crystallization, phase separation, self assembly, and electronic transport. Advances in AFM technology, particularly high-speed and high-resolution imaging, enable investigation of polymer structure, function, and dynamics in real world conditions and across a range of relevant spatial and temporal scales. In this perspective, we highlight a collection of recent polymer studies that utilize AFM to correlate the function and structure of polymer films, with focus on its multiparametric imaging capabilities. As the complexity of polymer materials and morphologies continues to increase, AFM is well poised to meet the accompanying demand for nanoscale imaging and characterization.

KEYWORDS
atomic force microscopy, nanoscale characterization, polymer dynamics, polymer structure, thin films

1 | INTRODUCTION

Due to their remarkable material flexibility, polymers have found widespread use in many contemporary fundamental and technological applications. Polymer structure and function depend hierarchically on their chemistry and chain architecture, as well as their organization and aggregation.[1] Structural organization occurs over a hierarchy of length scales, ranging from the conformational packing of individual chains to the self-assembly of mesoscale patterns. Similarly, polymer dynamics span a range of time scales, from rapid single-chain reptation to slow bulk diffusion and mass transport. This multiscale material heterogeneity yields emergent and application-specific functionality. As new and increasingly complex polymer materials are continually designed, imaging methods must meet the challenge of correlating local structure and function over the full breadth of relevant structural and dynamic properties.

In this Perspective, we examine the contributions of atomic force microscopy (AFM) toward addressing key developments in polymer science. The multiparametric imaging capabilities of AFM make this technique particularly useful for investigating the structure, dynamics, and functionality of polymer surfaces and interfaces.[1–3] We follow in the footsteps of an excellent recent review by Wang and Russell.[3]

Alongside AFM, many nanoscale imaging techniques have been employed to understand the structure and function of polymer materials, with electron microscopy (SEM and TEM) and X-ray scattering (SAXS and GISAXS) methods, being among the most commonly used.[4–6] While electron microscopy offers fast scan rates and high resolution, polymer samples are generally sensitive to damage from the electron-beam exposure, precluding dynamic measurements of a single region. Additionally, polymers often require pretreatment (e.g., staining, mineralization, or encapsulation) to enhance contrast and stability.[7,8] Requisite compatibility with a vacuum chamber also limits the capacity for in situ environmental control in SEM or TEM measurements. As complementary methods, X-ray scattering experiments, that is, small-angle X-ray scattering (SAXS) and grazing incidence small-angle X-ray scattering (GISAXS), reveal mesoscale ordering and phase transitions in polymer systems.[9,10] Reciprocal space measurements provide bulk information averaged over the sample or, for GISAXS, averaged over the film surface. Most X-ray scattering experiments still rely on synchrotron radiation, narrowing instrumental access. Lastly, both electron microscopy and X-ray scattering measurements are typically limited to obtaining only structural information, requiring external acquisition of functional properties. AFM stands out for its unrivaled capability to study a wide breadth of structural and dynamic features nondestructively in real space and time, and in a variety of application-relevant conditions.

Since its development 35 years ago, AFM has proven to be a powerful and flexible tool for characterizing nanoscale materials.[11,12] Over time, this initially revolutionary advancement has become part of the everyday toolkit for polymer scientists, transforming our understanding of nanostructure and processes. New advances in AFM imaging have successfully overcome a series of traditional limitations; these developments have been catalogued in detail in References 13–17. Although the focus of this Perspective will predominantly be on synthetic polymer systems, many of the key developments have been the result of efforts studying biologically-derived polymers.[13,16,18–20] The mission to capture biological mechanisms and dynamics in real time and under physiologically relevant conditions have highlighted the demand for gentle, nonperturbative imaging, fast scan rates, and imaging in liquid environments. These same methods have also been applied to answer critical questions in synthetic polymer systems. Among these developments, high-resolution, high-speed, and environmentally controlled AFM, in particular, have expanded the scope of functionality that can be understood at the local scale: high-resolution imaging captures the structure of single molecules; high-speed AFM has transformed the ability to track dynamics in real-time; and environmentally controlled AFM has enabled simulating real-world conditions in situ.

In this perspective, we highlight a collection of recent advances in AFM imaging with a focus on the potential applications of synthetic polymeric materials. We first introduce AFM along with a few of the key modes and capabilities that have enabled characterization of polymer function alongside imaging. We then examine the contributions of AFM to a range of topics in polymer science: crystallization, self-assembly, polymer electronics, transport, and solvation. The versatility of AFM has unlocked new and ongoing potential for uncovering structural, dynamic, and functional properties of polymers.

2 | AFM METHODS FOR POLYMER ANALYSIS

AFM is a scanning probe technique that measures the force between the tip of a cantilever probe and a sample surface. It was first developed by Binnig, Quate, and Gerber in 1986, extending the scope of scanning tunneling microscopy to non-conductive samples.[11] Since their invention, AFM systems have become more advanced

but the underlying principles remain the same. The AFM probe, consisting of a force-sensing cantilever equipped with a sharp nanoscale tip, is brought in contact with, or in proximity to, the sample surface. As the probe is scanned over the region of interest, variations in the cantilever's response are used as feedback to control the tip-sample separation and maintain a consistent interaction force. In this manner, AFM imaging may be used to directly interrogate the sample's topography and nanomechanical response. This force-measurement scheme can be further generalized to study a wide range of surface attributes and map local heterogeneities in the electronic, magnetic, optical, or electrochemical properties of a sample.[3] This multiparametric capability of AFM enables its unique ability to correlate surface structure and functionality.

A particularly valuable feature of AFM is its amenability to a wide range of sample environments, including ambient, vacuum, and liquid environments that simulate real-world operational conditions.[21] It can be used in an oxygen- and water-free glovebox, as well as under controlled humidity or solvent-vapor conditions relevant to polymer processing.[22,23] The AFM stage can also be heated to observe dynamics or high-temperature phase transitions or cooled to promote stability.[24–26] Fluid-cell imaging in which the sample and AFM probe are immersed in an aqueous solution has long been used for biological samples and has been extended to other polymer systems. This method can help with sample preservation and imaging stability, while also replicating physiological conditions.[27]

Advances in AFM imaging have helped to build on its natural strengths and to overcome its traditional limitations. Improvements in noise stabilization have enhanced AFM's sensitivity and spatial resolution such that commercial AFMs are now frequently used to resolve molecular features.[14,20]

2.1 | Imaging modes

The wide variety of AFM imaging modes makes it an all-in-one tool for polymer characterization. In the simplest imaging scheme, the tip stays in contact with the surface (contact mode) and the feedback loop ensures a constant cantilever deflection. In amplitude-modulated AFM (tapping mode), the tip is oscillated at or near its fundamental resonant frequency, and the amplitude of the oscillations is used to monitor the sample interaction. Intermittent contact with the sample reduces lateral forces in order to minimize damage to the tip and sample.[14] As another benefit of tapping mode, measurements of the phase offset between the oscillating drive frequency and cantilever response correspond with energy dissipation at the tip.[28] Phase imaging is particularly useful for studying polymeric systems where phase is associated with viscoelastic damping and can be used to map compositional or structural variation of the polymer surface.[29] However, the phase signal depends on a complex combination of dissipative and conservative interactions and is even susceptible to contrast inversion, making interpretation difficult. New methods of relating phase to real surface properties, has facilitated direct and quantitative viscoelastic measurements.[30,31] As one example, loss tangent mapping, derived from AFM phase imaging, measures the ratio of dissipative and conservative tip-surface interactions. As shown in Figure 1, such mapping can be used to distinguish the structural and compositional heterogeneity of a polymer blend during in situ crystallization.[31]

Quantitative measurements of polymer material properties can also be performed through a variety of nanomechanical imaging modes.[17] With off-resonant nanomechanical mapping, the cantilever is oscillated at a lower frequency in order to capture complete force-distance curves on each oscillation cycle. Additionally, multifrequency AFM, in which the cantilever is simultaneously excited at multiple resonances, allows for the concurrent acquisition of multiple parameters for decoupling the sample's intrinsic material properties from the tip specific interaction. Each excited mode can be maintained through different feedback channels or left open according to the experimental design.[15,32,33]

Advanced imaging modes utilize AFM's force-sensing capabilities to image a variety of functional properties. These modes are often coupled with application-specific cantilevers. For example, in conductive AFM (C-AFM), current flow between the sample and a metallic or metal-coated cantilever is used to map variations in electrical conductivity.[34] In Kelvin probe force microscopy (KPFM), tip bias is controlled to minimize mechanical oscillations and match the sample's surface potential.[34,35] In AFM-IR modes, a metallized probe acts as an antenna to locally amplify the spectroscopic signal for sub-diffractive imaging. These methods measure changes in either sample polarizability and thermal expansion (photo-induced force microscopy, PiFM) or in the tip-scattered light (scattering scanning near-field optical microscopy, s-SNOM) as a function of excitation wavelength.[36,37] In electrochemical AFM (EC-AFM), the probe is used to monitor redox chemistry of samples immersed in an electrolyte solution.[38] For these measurements, a conductive probe is coated in an insulating sheath exposing only the tip apex to ensure sensitivity to local reactivity. These modes represent just a few of many functional imaging capabilities, and with any of these techniques,
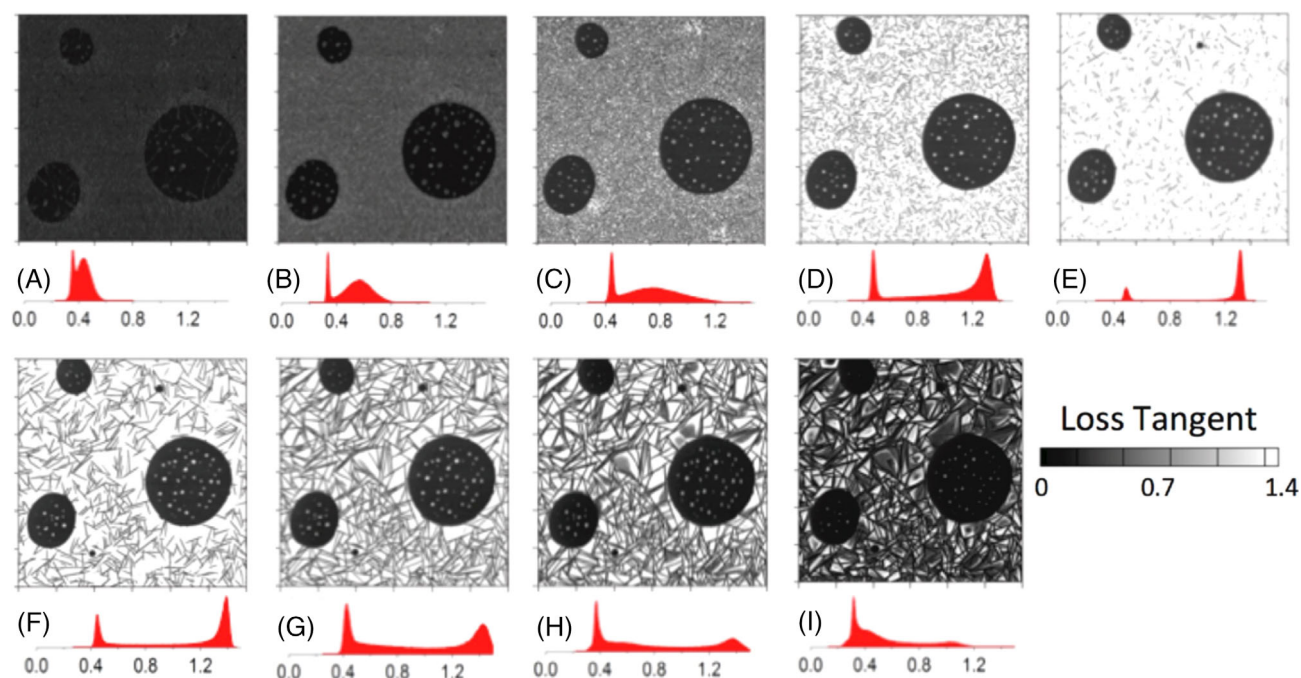
FIGURE 1 Atomic force microscopy (AFM) loss tangent images throughout an in situ heating experiment of a polymer blend film with a continuous phase of PP surrounding PS domains. The images were acquired as the film was first heated to (A) 55°C, (B) 80°C, (C) 100°C, (D) 120°C, and (E) 135°C, and then cooled to (F) 120°C, (G) 100°C, (H) 80°C, and (I) 55°C. Nanomechanical contrast of the loss tangent images tracks both the compositional differences as well as the structural evolution of the PP phase during crystallization. Reproduced with permission from Reference 31. Copyright 2016, AIP publishing LLC

multiparametric imaging allows direct correlation with the local surface topography or other properties.

2.2 | High-speed AFM

The development of high-speed AFM (HS-AFM) has opened up the possibility of imaging dynamic samples in real time with minimal interference from the imaging method. Imaging time-resolution has improved dramatically for real-time observation of dynamic processes, reflecting a remarkable transition from timelapse (multi-minute) to video rate (subsecond) imaging. HS-AFM advancements were largely initiated from biological studies, in which there was a desire to image at rates fast enough to capture dynamic biological processes, while also having the ability for non-destructive, label-free, and physiologically relevant imaging conditions. The development of this technique required advancements in nearly all components of traditional AFMs, including cantilevers, cantilever excitation methods, deflection measurement, scanners, and controllers, and subsequent commercialization of these ongoing developments has increased the accessibility of HS-AFM.[39–52]

One of the more notable accomplishments of HS-AFM is the elucidation of the translocation mechanism

or walking of myosin V along actin filaments by Kodera et al., in which the authors used HS-AFM to capture the dynamic conformational changes in the protein in real time.[53] High-speed imaging has continuing relevance for polymer samples, including crystallization, polymerization, diffusion, and mesoscale self-assembly.[54–58] Recently, Kretzmann et al. used HS-AFM to directly observe polymer dynamics at a liquid–solid interface, replicating physiological conditions, to better understand the role of polymers in biomedical delivery applications.[59]

2.3 | Subsurface imaging

The functionality of many polymer systems depends not only on their surface, but on the nanostructural organization buried within their three-dimensional (3D) volume. While AFM is conventionally considered to be sensitive to only surface and near-surface regions, advancements in imaging methodology and theory have unlocked the potential for subsurface imaging.[60] In subsurface imaging modes, tip-sample interactions are influenced by the full volume underlying the contact point and consequently reflect a convolution of surface and subsurface properties. Decoupling these interactions is not obvious, and careful approaches are necessary to reconstruct a 3D map from a

two-dimensional (2D) scan. In particular, imaging contrast in heterogeneous materials is dependent on both the depth and the physical contrast of subsurface features, and complete reconstructions must differentiate between these factors. A wide range of subsurface imaging modes have been developed, including nanomechanical, acoustic, and optical methods.[60] In polymer films, these methods have been used to map the organization of buried polymer crystallites and nanoparticles and to measure the depth of stacked multilayer films.[61–63]

2.4 | Force spectroscopy

In addition to imaging modes, the AFM tip can be used to measure tip-surface interactions as a function of sample distance.[64] In nanoindentation experiments, the probe is repeatedly depressed into a compliant sample surface to measure its viscoelastic response. The probe can also be used to "fish" individual polymer chains and measure their extension as the cantilever is retracted. The resulting force-distance spectra contain rich material information on local elasticity, hardness, and adhesion. All force spectroscopy data must be coupled with nanomechanical modeling to determine these rheological properties. Local force measurements can be used to relate the mechanical properties of single polymer chains to bulk continuum properties.[65]

2.5 | Scanning probe lithography

Alongside its characterization capabilities, the AFM nanoscale probe can be used to lithographically manipulate a sample surface.[66,67] Increasing the tip-sample interaction force can transition from a non-perturbative imaging mode to a lithographic mode that purposefully deforms, removes, or otherwise alters the scanned region.[68] Scanning probe lithography (SPL) is well-suited for the direct patterning of nanoscale features in polymer films.

In the simplest application of SPL, the scanning action is used to mechanically scratch or plow the polymer surface.[69] Alternative lithographic approaches take advantage of the ability to locally modify tip properties: thermal probes can be used to locally induce crystallization or mass flow in polymer samples and conductive probes can generate electric fields for manipulating charged samples.[70,71] In dip-pen lithography, the tip is coated in a fluid material, which it deposits (writes) by tracing over the surface.[72] Each of these methods is well-suited for the modification of polymer films due to their responsiveness and adaptability. While raster scanning limits throughput of SPL, the development of multiple tip write arrays has increased lithographic efficiency.[73]

3 | POLYMER APPLICATIONS

3.1 | Crystallization

More than half a century of intensive experimental and theoretical progress has served to advance our understanding of polymer crystallization.[74,75] Along the way, AFM has contributed significantly to these efforts, with direct real-space imaging helping to resolve debates and to inspire the development of new crystallization models.[3,76] Still, many key questions remain unanswered and polymer crystallization has been highlighted as a top remaining challenge in polymer physics.[75,77]

Below the equilibrium melting temperature, semicrystalline polymers adopt a metastable morphology including both crystalline and amorphous regions. In these systems, polymer chains fold into crystalline lamellar sheets with nanoscale thicknesses interposed with amorphous layers. On the mesoscale, lamellae further organize into a diverse array of structures, including single-crystal platelets, branching dendrites, and space-filling spherulites. The morphology and degree of crystallinity in semicrystalline systems is dependent on the sample's processing history as limited by crystallization kinetics. For any of these forms, structural heterogeneity also leads to local variation in polymer properties and functionality.[76]

Key features of folded chain crystallization are captured by secondary nucleation theory, developed by Hoffman and Lauritzen, which describes the attachment of polymer stems at the crystal growth front.[78] This model is based on a single-step growth process in which a sharp capillary interface separates crystalline and amorphous regions. However, AFM observations of the formation of lamellar crystallites challenged these assumptions. Following crystallization from the melt, syndiotactic polypropylene lamellae exhibit a knobbled texture indicative of a multistage crystallization process in which discrete crystal subunits fuse to form lamellar sheets.[79] In measurements of spherulite formation in bisphenol A, AFM phase images identify a region with gradually shifting contrast at the growth front between crystalline and amorphous regions.[80] Consistent with these observations, a multistage crystallization theory, developed by Strobl, introduced an intermediate mesomorphic region in which polymer chain organization and mobility change continuously when approaching the growth front.[81]

Advances in AFM imaging stability have enabled measurements of the lamellar substructure and growth

processes with molecular and submolecular resolution. Kumaki et al. first observed the characteristic folded-chain structure in 2D isotactic PMMA crystals prepared through the slow compression of a monolayer Langmuir–Blodgett film and deposited on mica.[82] More recently, humidity-induced crystallization of isotactic PMMA has enabled in situ observations of nucleation and growth processes with molecular resolution.[83] The crystals exhibited stepwise growth kinetics, potentially due to the attachment of discrete polymer chains and further indicative of a multistage crystallization process. The evolution of crystal shapes revealed significant chain mobility and cooperative slipping even within aligned lamellae. In separate experiments, high-resolution imaging of 2D P3DT crystals on hBN also clearly resolved the folded-chain structure of the polymer backbone as well as faint contrast of the perpendicularly oriented decyl side chains, Figure 2A-C.[84] The packed crystalline stems fold in place, connected by tie-chains with sharp hairpin bends. To further improve imaging sensitivity, measurements using a small oscillation amplitude and the third cantilever eigenmode distinguished individual sulfur atoms within the thiophene rings, as identified by the extended size of the sulfur lone-pair, Figure 2D. The P3DT lamellae were found to orient with three-fold symmetry, guided by epitaxial alignment of the alkane side chains with the hBN substrate. This contrasts with observations of isotactic PMMA on mica, which showed only partial alignment with the substrate lattice. Instead, the orientation was

determined during the initial nucleation step and reinforced through subsequent coarsening.[83] In substrate confined systems, a balance of epitaxial and interchain interactions must be accounted for in understanding crystal organization.

Molecular resolution has also been achieved outside of 2D, surface-confined polymers. AFM imaging has visualized the lattice structure of P3HT crystals at the surface of a spin-coated film, in which π-π stacking of the thiophene backbones leads to alignment of hexyl chains in a square lattice normal to the surface plane.[84] With high-speed AFM imaging, Acevedo-Cartagena et al. observed the real-time surface nucleation of P3HT nanofibers from a supersaturated solution. Phase imaging of the nanofibers tracked their growth and clearly resolved crystalline packing of the backbone and hexyl side chains in alignment with the nanofiber axis.[85]

Chain-packing interactions within a crystal can be measured through single-molecule force spectroscopy. With finite probability, contact between the AFM probe and a polymer crystal leads to physisorption of an individual chain. As the chain is drawn from the crystal lattice, periodic peaks in the force-extension spectrum correspond with the removal of each complete fold, as shown in experiments with PA in Figure 3A,B.[86] The magnitude and substructure of each peak further reveal the nature of chain packing interactions, Figure 3C,D. Stick–slip profiles result from incremental breaking and reformation of hydrogen bonds at each repeat monomer
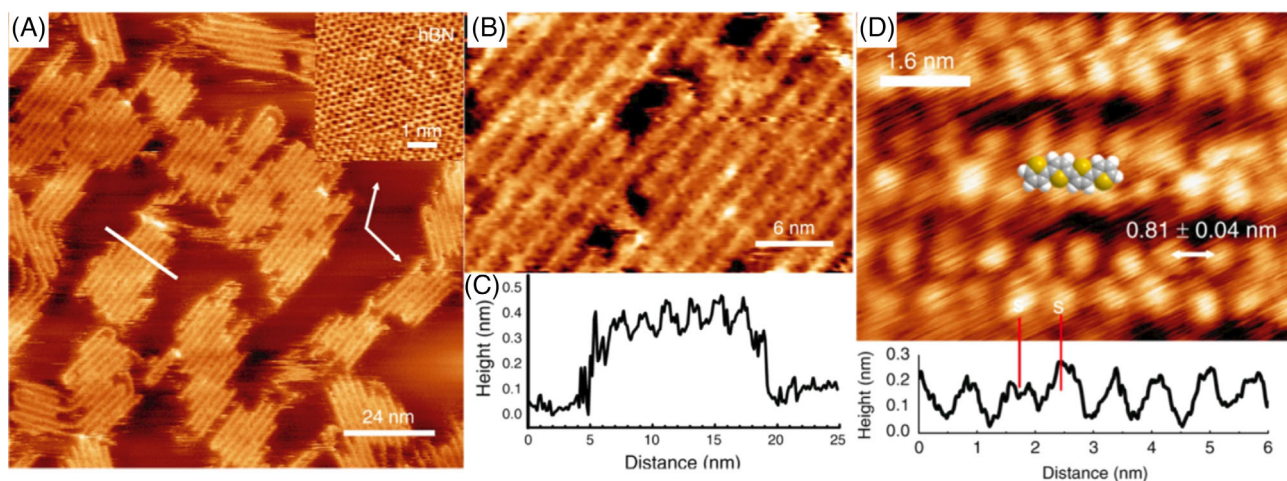

FIGURE 2 High-resolution tapping mode height images of two-dimensional P3DT adsorbed on the surface of hexagonal boron nitride (hBN). (A) The folded-chain lamellar structure is clearly visible in the topographic image; the inset shows a lattice frequency shift image of the hBN substrate. Three-fold orientational symmetry of crystalline domains is due to epitaxial alignment with the hBN lattice. (B) A selected area from scan (A) shows the organization of individual PT molecules and orthogonally-oriented low-contrast features associated with decyl side chains. (C) A height profile along the line in (A) shows a molecule-to-molecule separation of 1.95 ± 0.02 nm. (D) An AFM height image acquired using the third cantilever eigenmode resolves features associated with individual sulfur atoms in the P3DT chains with 0.81 ± 0.04 nm interatomic spacing. Adapted under Creative Commons from Reference 84. Published by Springer Nature

FIGURE 3 (A) Scheme of a single-chain pulling experiment from a single crystal. Adapted with permission from Reference 87. Copyright 2019, American Chemical Society. (B) Force extension curves of PA chains have periodic structure corresponding to the unraveling of successive polymer folds. (C) Schematic showing hydrogen-bonding interactions between adjacent polymer chains within the lattice. (D) the substructure of each peak shows stick–slip motion due to iterative breaking and reforming of these hydrogen bonds between monomer units. Adapted with permission from Reference 86. Copyright 2018, American Chemical Society
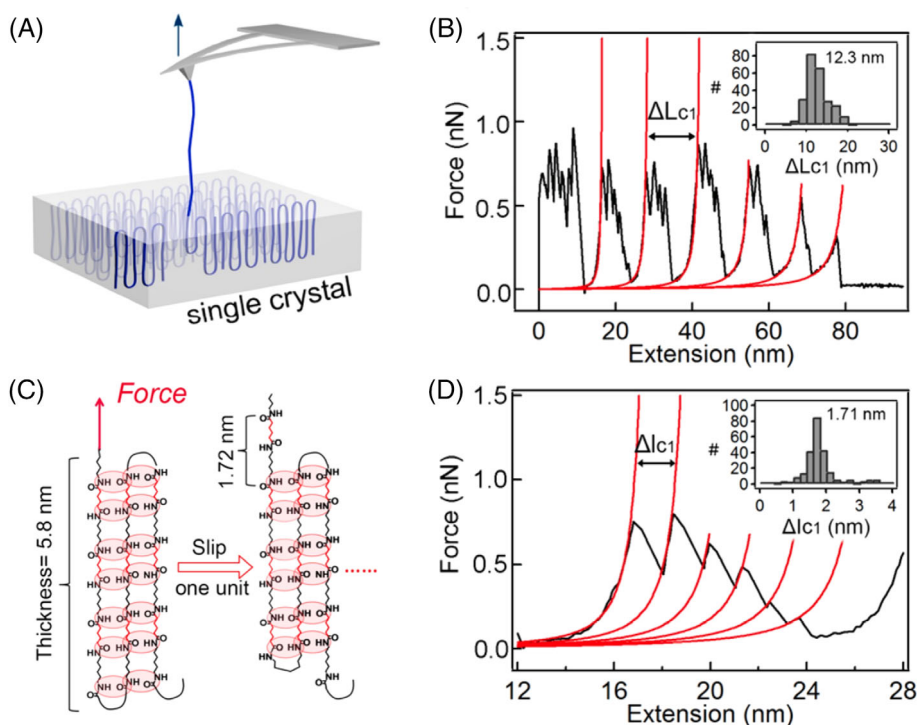
unit. Similar stick–slip motion, albeit with lower magnitude forces, is observed in PCL crystals, in which chains are stabilized through electrostatic dipole interactions.[87] In contrast, PEO and PLLA chains, which adopt a helical chain conformation, instead show continuous unraveling of each lamellar fold.[87,88]

3.2 | Block copolymer self-assembly

Block copolymers (BCP) have garnered attention from academia and industry for their ability to self assemble into periodic nanoscale patterns with features sizes smaller than can be obtained through traditional lithographic methods.[89,90] The periodic structures adopt a variety of stable morphologies, including lamellae, cylinders, or spheres, depending on the relative volume fraction of the blocks.[91,92] However, lack of directional preference for alignment limits long range ordering and produces defect-dense fingerprint patterns, as shown in an AFM phase image of cylinder-forming PS-b-PMMA in Figure 4A. There has been a concerted effort to guide the self assembly process in order to control the orientation and organization of the patterns. Ordering can be achieved through external guiding fields (e.g., electric fields, solvent flow, strain) that break symmetry and ensure a preferred pattern orientation. Alternative strategies have focused on directed self assembly through lithographic substrate patterning under two broad categories: (1) graphoepitaxy, which modifies the substrate

topography,[93] and (2) chemoepitaxy, which modifies the substrate chemistry.[94] In each case, the periodicity of the lithographic pattern is multiplied by the BCP self-assembly process to produce patterns with finer resolution than achieved through top-down methods alone.[90] An example of graphoepitaxy, again with cylinder-forming PS-b-PMMA, is shown in Figure 4B before and after alignment. In addition to fully aligned systems, the formation and location of dislocations can be further controlled by the channel geometry, as with tapered channels in which the width varies continuously. Dislocations form at regularly spaced sites where the channel width does not accommodate an integral pattern spacing, shown in Figure 4C. With in situ AFM imaging, tracking the motion of individual dislocations allows for controlled measurements of defect energetics and diffusivity.[95]

The intricate patterns produced by BCPs have inspired AFM imaging from early in its development.[96] Real-space images of BCP morphology served as direct confirmation of its structure as predicted theoretically and measured in reciprocal space through X-ray and neutron scattering experiments.[91] AFM phase imaging, as shown in Figure 4, measures differences in the viscoelastic properties of the BCP components to produce a compositional map. In combination with topographic imaging, phase images are routinely used to relate the microstructure to various material parameters, including composition, molecular weight, film thickness, and interfacial interactions.[92,97] In addition to elucidating the
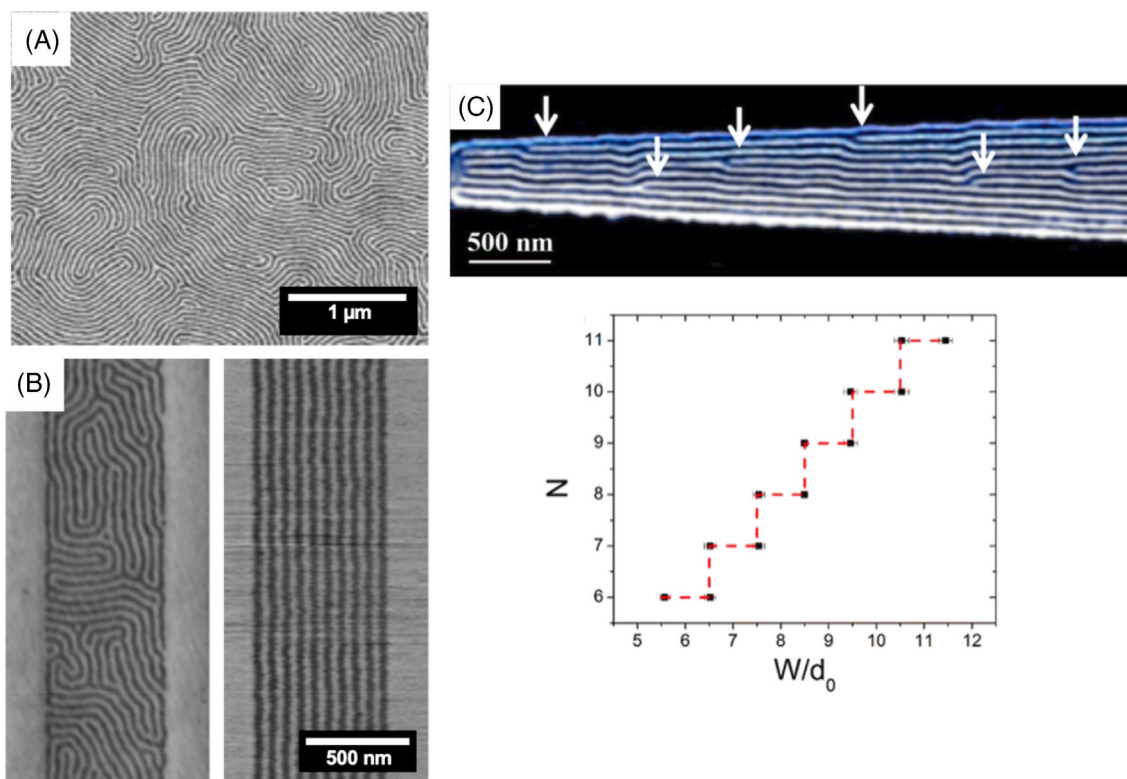
FIGURE 4 (A) Atomic force microscopy (AFM) phase image of cylinder-forming block copolymer in a fingerprint pattern. The block copolymers (BCP) in this image is PS-b-PMMA. (B) AFM phase images illustrating the graphoepitaxy process with cylinder-forming PS-b-PMMA. The cylinders preferentially align with the channel sidewalls, propagating linear alignment throughout the polymer upon thermal annealing. (C) Representative images showing confinement of PS-b-PMMA in annealed tapered-width channels. Dislocations, indicated with white arrows in the AFM phase image, occur at regular intervals along the length of the channel, as shown in the plot of number of cylinder domains, N, versus the confinement width, W, in terms of equilibrium periodicity, d_0; the black dots represent the dislocation positions. Adapted with permission from Reference 95. Copyright 2014, American Chemical Society

surface morphology, subsurface imaging of BCP patterns has been used to map the 3D structure of embedded cylinders, distinguishing depth information from the materials' mechanical contrast.[61,98]

Beyond structural characterization, the AFM environment can be controlled to replicate BCP processing conditions—including solvent-vapor annealing (SVA), direct immersion annealing (DIA), and thermal annealing—and track pattern evolution. The presence of solvent vapor plasticizes polymer films while also swelling the BCP domains and mediating block interactions. During SVA, polymer films therefore freely reorganize to adopt a new equilibrium morphology as defined under solvent swollen conditions.[99–101] However, measurements of the quenched state following SVA are complicated by chain collapse, gradients in solvent flow, and surface dewetting upon solvent removal. For example, Zhang et al. showed that thermally annealed PS-b-P2VP films with cylinders, initially oriented perpendicular to the substrate, exhibit dewetting after SVA, with parallel cylinders near the dewetted regions. After SVA for 24 h, the

parallel alignment propagates across the film, as the cylinders align with the moving contact line at the edge of a dewetted region.[102] Environmental AFM imaging offers the potential to image these annealing processes in situ, capturing the annealing dynamics and mechanisms in real time, as well as capturing the morphological changes that accompany deswelling of the polymer films. Takano et al. recently demonstrated in situ AFM imaging within a sealed SVA chamber, enabling direct measurements of solvent-swollen films. The system monitored the coarsening of fingerprint patterns in ultrahigh molecular weight PS-b-PMMA thin films over an 8 h period of in situ SVA imaging, shown in Figure 5.[103] DIA offers a method to overcome many of the challenges associated with SVA, fully immersing BCP films in a tunable solvent mixture, in order to maintain a finite interaction parameter for microphase separation.[104,105]

AFM imaging has been extensively used to study the dynamics and mechanisms of BCP defect healing and grain coarsening during thermal annealing. Harrison et al. first identified grain growth kinetics following a $t^{1/4}$
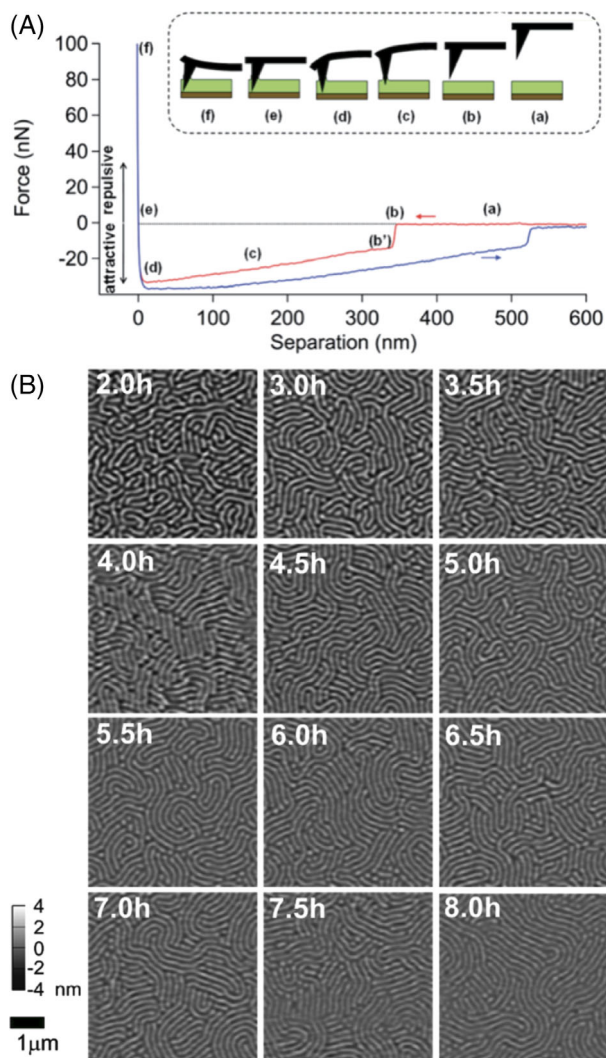
FIGURE 5 (A) Schematic illustrating force-distance measurements in solvent-swollen films, along with a representative force-distance curve used to determine the thickness of the swollen film. (B) Atomic force microscopy (AFM) topographic images of the solvent swollen films, showing the progression of the solvent-vapor annealing (SVA) in situ. Over the 8.0 h annealing time, the polymer domains coarsened and correlation length increased, while defect density decreased. Adapted under Creative Commons from Reference 103. Published by the Royal Society of Chemistry

was used to scratch the polymer film and its subsequent recovery was observed. The re-emergent BCP patterns were found to conform with the orientation of the neighboring undisturbed pattern.[112] Recent advancements in HS-AFM during thermal annealing have expanded the range of accessible BCP dynamics. High-speed imaging has been used to study the initial stages of microphase separation and lamellar formation from a spin-coated film.[113] It has also been applied to track the conversion of a metastable "stitched" morphology templated by a chemically patterned substrate (chemoepitaxy) to its final aligned geometry.[56,114] In these systems, scan rates are limited by the potential for sample damage of the heated polymer melts rather than the AFM imaging capabilities. In addition to measuring morphological evolution, high-speed, temperature-controlled AFM has been used to track fluctuations of the PS/PMMA interface of confined BCP cylinders in real time, shown in Figure 6.[115] Disabling of the AFM slow-scan axis allowed for rapid sampling of one-dimensional phase profiles to monitor equilibrium fluctuations of the interfacial boundary, sacrificing one spatial dimension for a dramatic increase in time resolution. Fluctuations of the cylinder edges, placements, and widths were found to be spatially coherent over multiple domains due to the chain connectivity and incompressibility of the blocks and were enhanced with increasing measurement temperatures.

Recent advancements in AFM-IR have achieved nanoscale chemical contrast of BCP patterns. With 10 nm spatial resolution, IR s-SNOM measurements of PS-b-PMMA were sensitive to sample volumes containing $\sim 10^4$ carbonyl oscillators. In these measurements, the PMMA carbonyl stretch was found to redshift at the center of PMMA-enriched domains due to the changing dielectric environment.[116] As a complementary method, PiFM imaging was used to generate complete multispectral maps of PS-b-PMMA and PS-b-P2VP patterns,[117] and has also been performed in combination with nanomechanical mapping, correlating chemical composition with nanoscale material properties.[118]

3.3 | Polymer electronics

Conductive polymers are useful for organic electronic devices due to their compatibility with low-cost and low-energy fabrication processes.[119] Among their applications, polymer-based systems can be used for solar cells, light-emitting diodes, memory storage, and bioelectronic devices. The active layer of these devices typically consists of a donor/acceptor blend with large interfacial areas to facilitate charge separation. The performance of these blends depends on their nanoscale morphology,

power law in striped fingerprint patterns, determined by the annihilation of topological defect structures.[106] Subsequent in situ studies of unconfined thin films elucidated the complex pattern evolution mechanisms involved in the annihilation process.[107,108] Confinement in lithographic channels provides a controlled environment for isolating individual defect pairs, allowing for direct measurement of the free energy landscape for defect annihilation pathways.[109–111] In situ thermal annealing has also been used to track self-healing and flow of polymer in response to mechanical damage. An AFM probe
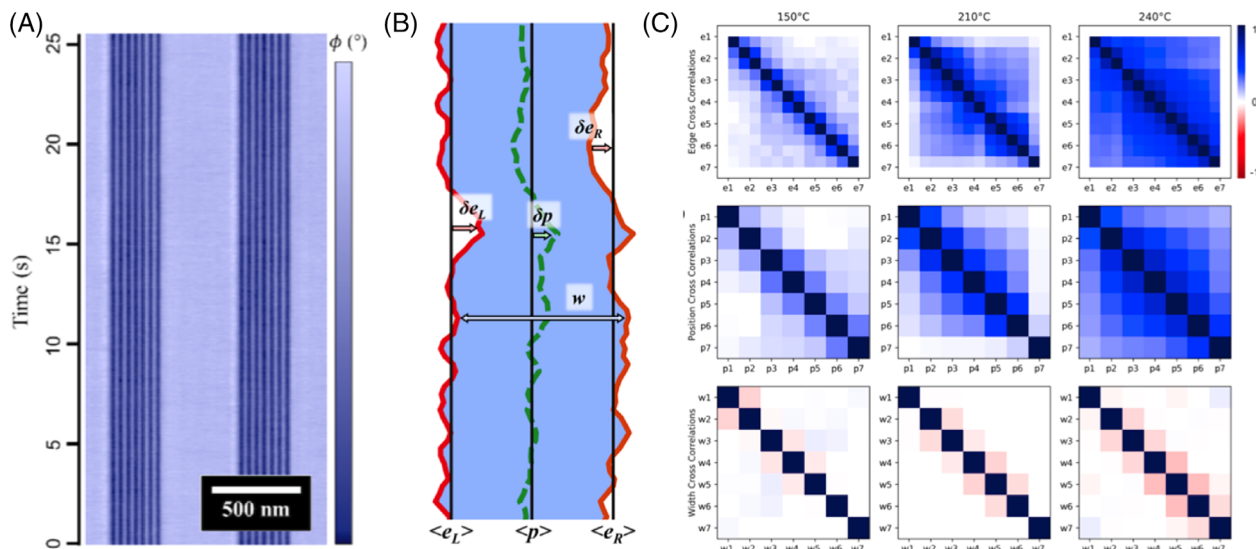
FIGURE 6 (A) Slow-scan disabled (SSD) atomic force microscopy (AFM) phase image of cylinder-forming PS-b-PMMA confined in lithographic channels. In SSD imaging, the *x*-axis is displacement and the *y*-axis is time, allowing direct tracking of the displacement of polymer cylinders in real time. (B) Schematic depiction of fluctuations of polymer cylinder edges ($\delta e_{L/R}$), placement (δp), and width (δw). (C) Pearson correlation coefficient plots showing coherence in cylinder fluctuations, propagating throughout the channel for edge and placement fluctuations, and anticorrelation for width fluctuations, extending only to adjacent cylinders. Reproduced with permission from Reference 115. Copyright 2019, American Chemical Society

including the domain size, domain connectivity, degree of separation and electrode contact area. In turn, the heterogeneous film structure is strongly dependent on its processing history. For example, blend films form different as-cast structures when deposited from different solvents.[120]

AFM topographic mapping alone is insufficient for characterizing these blend morphologies, as compositional domains can be observed as either concave and convex features even within the same image.[121] For this reason, electrical AFM methods are used to correlate functional material properties with the local material structure: C-AFM measures current flow through conductive pathways, providing information on through-film connectivity and local mobility; KPFM maps the surface potential, providing information on molecular energy levels and charge trapping; and photoconductive AFM (PC-AFM) measures current generated from light exposure.[34,119] Local mobility measurements often significantly exceed bulk mobility measurements obtained using parallel plate electrodes, as the 3D tip-substrate geometry samples current from an extended effective surface region. Corrections accounting for these space charge effects yield mobilities in good agreement with macroscopic measurements, but with nanoscale spatial resolution.[122]

By measuring current flow through polymer films, C-AFM can determine whether surface domains extend through the entire film thickness to the underlying electrode. Measurements of P3HT/PVDF-co-PTrFE blends found that at low P3HT loading, the majority of domains observed at the surface did not form conductive columns. Comparative KPFM measurements, which sampled the surface potential to a depth of 100 nm, of the same films mapped the subsurface domain connectivity. As the P3HT fraction was increased, domains formed large interconnected networks and correspondingly greater through-film conduction.[121] Similarly, Daviddi et al. found that, in blends of P3HT:PMMA, the P3HT forms conductive islands in a surrounding insulating PMMA matrix. The C-AFM measurements, shown in Figure 7, indicate that the conductivity of the islands is not uniform, with the larger domains tending to have a higher measured current.[123] C-AFM measurements show continuous conductivity gradients across domain boundaries, indicative of blend intermixing.[124] In polymer solar cells, the intermixed donor/acceptor region is important for charge generation, but has poor mobility and can also contribute to quenching.[120] The width of the boundary region narrows with increasing annealing temperature and more complete phase separation.[124]

Beyond structural characterization, with external illumination AFM can be used to measure photogeneration and degradation processes during device operation.[125] Significant variations in measured photocurrent have been observed within topographically indistinguishable domains.[126] Fluctuations in the photocurrent are associated with charge trapping and detrapping events in

FIGURE 7 Conductive AFM (C-AFM) (A) topography and (B) current images of P3HT: PMMA blend films of various blend ratios. Areas of higher topography correspond to areas of higher current, indicating the formation of conductive P3HT islands in an insulating PMMA matrix. Reproduced with permission from Reference 123. Copyright 2019, American Chemical Society
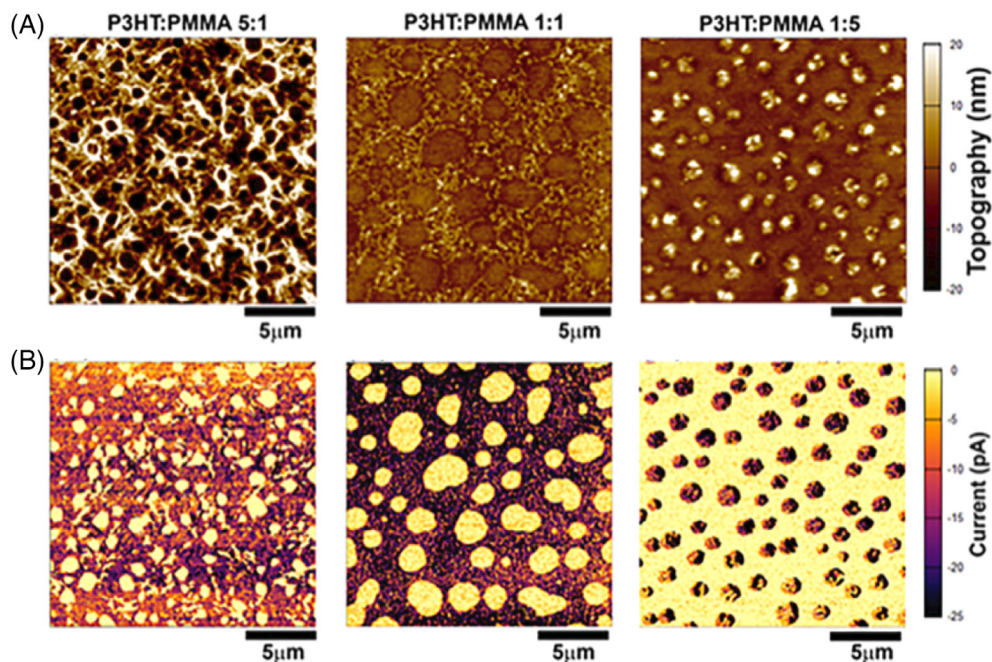
disconnected minority inclusions within phase-separated domains.[127] Combined heating and light exposure has been used to study photodegradation processes in polymer: fullerene blend films. These films undergo competing dimerization and decomposition (de-dimerization) processes when exposed to light and high temperatures, respectively. The AFM studies, shown in Figure 8, focused on PS:PCBM thin films as a model system and revealed that, above the glass transition temperature, pre-exposure to light reduces structural coarsening, indicating that the light-induced dimerization imparts stability to the system.[128]

3.4 | Membrane transport

To keep up with increasing demands for clean water, improvement in filtration methods is needed for water purification with improved energy efficiency, greater selectivity, and lower fouling. Polymer phase-inversion membranes are widely used due to their low cost and straightforward production. Next-generation membranes based on the self-assembly of block copolymers achieve narrow pore size distributions, high porosities, and controllable surface properties and chemistries. The synthesis of these membranes is beyond the scope of this perspective, but several recent reviews cover this topic,[129–132] as well as many literature examples.[133–140] AFM is commonly utilized to nondestructively characterize membrane topography, including pore size, shape, and size distribution, at a local level, as well as to understand membrane behavior in solvent environments.[141–143] In addition,

AFM phase imaging has been used to determine the relative hydrophobicity or hydrophilicity of a membrane sample[144] and to distinguish between new and fouled membranes.[145]

Further advances in AFM techniques offer the potential to gain insight into the behavior of membranes in environments that mimic their operating conditions. In particular, combining scanning electrochemical microscopy (SECM) with AFM offers the unique ability to characterize polymer membranes, including localized sensitivity, flux, and fouling. SECM, first introduced by Allen Bard in 1989,[146] is a scanning probe technique that measures local surface electrochemical properties by monitoring redox reactions at the imaging probe. A major limitation in SECM imaging is that the tip is held at constant height as it scans the sample surface, such that the resulting measurements are a convolution of current and topography. Combined SECM-AFM was subsequently introduced[147] to decouple these signals.[148–150] This combined imaging technique has been demonstrated as a method for imaging porous surfaces and membranes, as well as measuring transport through membranes.[151,152] The work of Gardner et al. in particular highlights the potential value in using SECM-AFM to characterize membranes in situ. They investigated iontophoretic transport through track-etched polyethylene terephthalate (PET) membranes and saw that not all pores identified in topography images contributed to ion transport and found significant transport heterogeneity across active pores, highlighting the added value of localized transport measurements.[153]
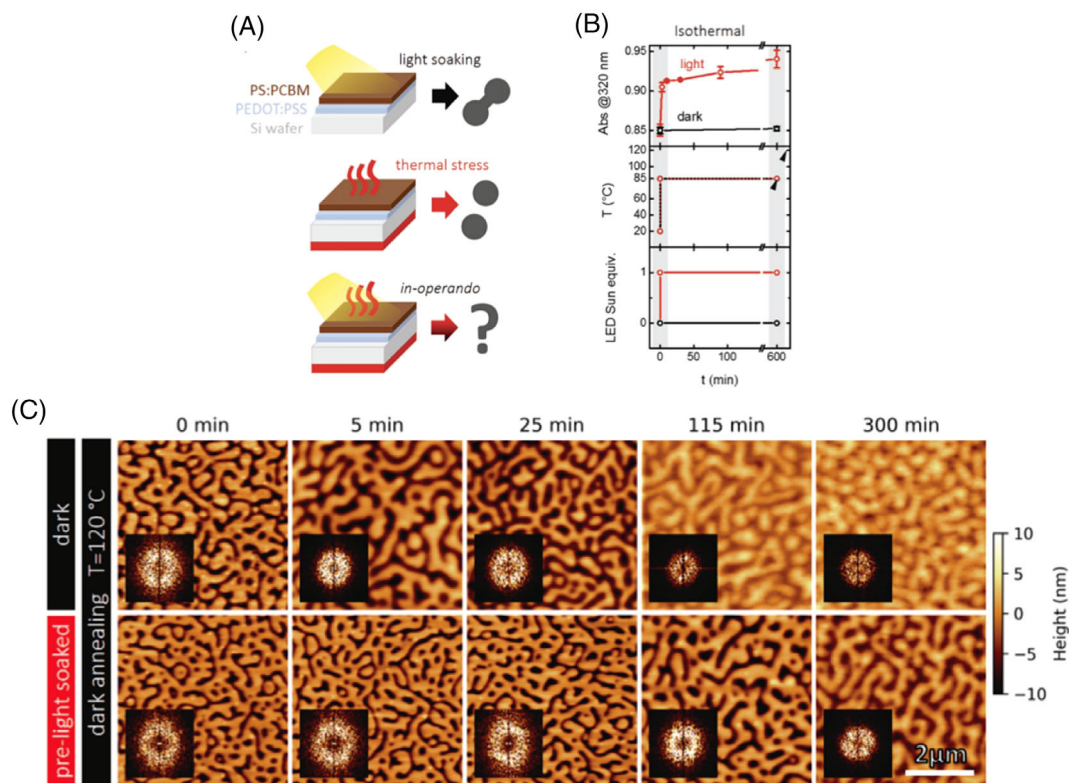
FIGURE 8 (A) Schematic illustration of the experimental setup to investigate the impact of light on polymer: Fullerene blends in (B) isothermal imaging conditions with (red) and without (black) pre-illumination. (C) AFM topography images of polymer blend films annealed at 120°C over time, with and without pre-illumination. Films not previously illuminated (top row) have rapid coarsening, while pre-illuminated films (bottom row) exhibit limited structural coarsening in the same period of time. The 2D Fourier transform insets indicate a spinodal structure.[128] Adapted under Creative Commons from Reference 128. Published by WILEY-VCH Verlag GmbH & Co

3.5 | Solvation and swelling

Many polymer applications, including drug delivery, lithographic etching, and molecular signaling, require the use of polymer films or brushes in liquid environments. However, when submerged in liquid, the polymer matrix swells, altering the polymer morphology, ordering, and self-assembly, particularly if the system is a BCP or polymer blend with differential solvent compatibility. Solvent-responsive polymers can be engineered to utilize these changes for desired functionality. Deswelling of the polymers after removal from the solvent can further alter the surface structure as the swollen chains collapse and enter a kinetically trapped state. The ability to image in liquid environments makes AFM a particularly powerful tool for investigating native swelling dynamics as well as programmed responses.

Lai et al. investigated polyacrylamide (PAAm) hydrogels to validate the use of Flory-Huggins theory, which describes the thermodynamics of polymer mixing, for modeling swollen polymeric materials.[154,155] They used dynamic oscillation indentation AFM to measure various

poroelasticity metrics (including shear modulus, Poisson's ratio, and diffusivity) submerged in aqueous polyethylene glycol (PEG). These experiments showed that the large volume change and accompanying stretching of the polymer chains renders Gaussian statistics insufficient to model stretched chains in swollen polymer films, and demonstrated that the deformation mechanism cannot be fully explained by Flory-Huggins theory. The authors proposed a series of equations to modify the swelling model and explain the observed behavior.[156] Our lab has used in situ AFM to investigate the swelling of terraced PS-b-PMMA thin films when submerged in cyclohexane. Solvent was observed to infiltrate along step-edges and propagate uniformly through polymer terraces. Solvation kinetics were limited by relaxation of the glassy polymer chains at the swelling front, as shown in Figure 9.[157] In addition to impacting the ordering or phase separation of polymer films, solvent-induced swelling can also lead to degradation of the polymer backbone. Messmer et al. investigated the solvation-induced main-chain scission in dendronized polymers, utilizing AFM topography along with molecular dynamics simulations to decipher the
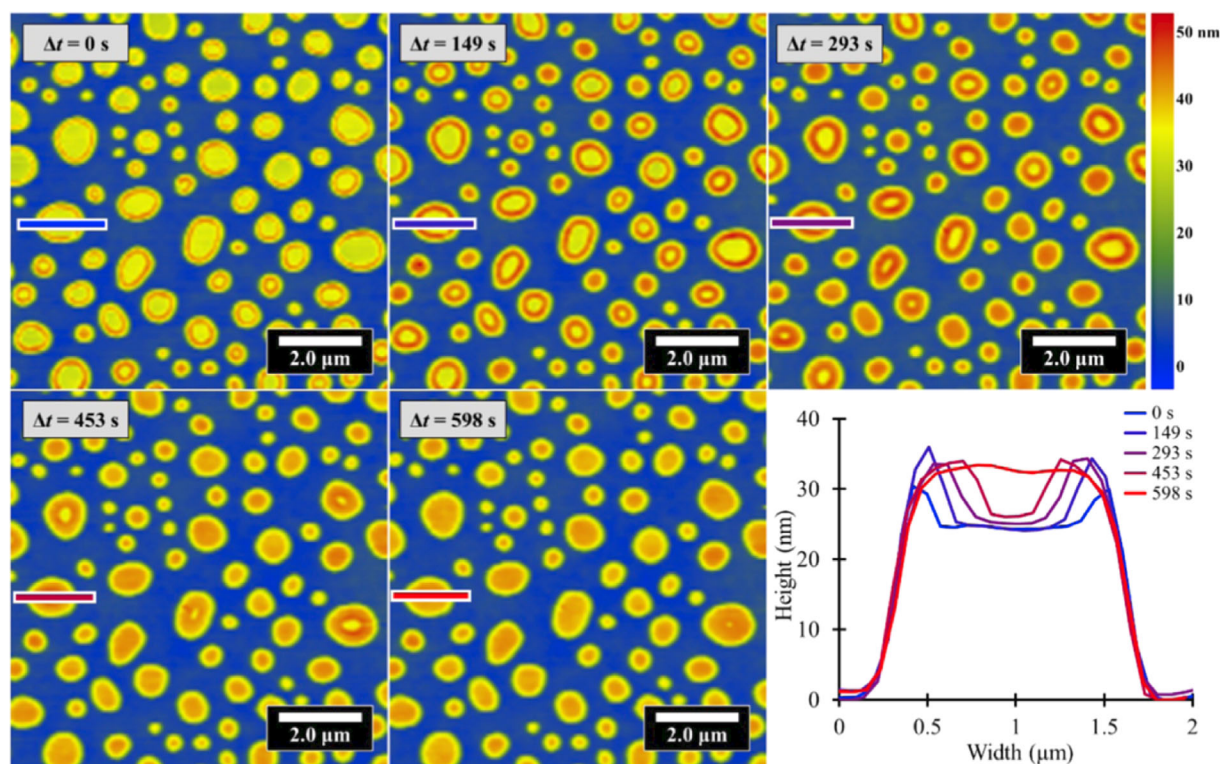
FIGURE 9 Time series of PS-PMMA islands immersed in cyclohexane tracking the solvation process. A sharp swelling front separating the solvent-swollen melt from the unsolvated glass propagates from the island edges. Height profiles show the time-evolution of island swelling. Reproduced with permission from Reference 157. Copyright 2019, American Chemical Society

scission mechanism in charged and neutral dendronized polymers. They find that solvent-induced scission is due to sterically induced degradation, that is internal mechanical stress caused by swelling in the dendritic periphery, as opposed to external stressors (e.g., reactants, temperature instability, etc.).[158] These findings provide further evidence that dendronized polymers can be thought of as colloidal particles, rather than classical linear polymers, in solution.[159]

Controlled polymer swelling can favorably alter the morphology and functionality of polymer films, for example altering the surface roughness or adhesive properties. Jalili et al. demonstrated that the roughness of polymer brushes can be manipulated by exposing the brush to good or poor solvent environments. They imaged morphology changes in PHEMA brushes on PDMS substrates when the substrates were submerged in water and cyclohexane, good and bad solvents, respectively. When exposed to a good solvent, AFM imaging revealed a swollen needle-like morphology structure with a uniform surface roughness, while exposure to a poor solvent led to collapse of the polymer film and a carpet-like morphology. Additionally, the PHEMA brush becomes more hydrophobic when exposed to varying degrees of ultraviolet/ozone treatments and the surface roughness

decreases with longer exposure times.[160] Controlled polymer swelling also has important implications for creating antifouling surfaces in relation to marine applications, e.g. preventing barnacle adhesion on ships.[161,162] A recent paper in this area utilized colloidal AFM-based force spectroscopy to investigate the response of methacrylamide- and styrene-based sulfobetaine polymer brushes, PSBMAm and PSBVB, respectively. Comparison of the nanomechanical and adhesive properties in water, salt water, and deuterium water revealed that the methacrylamide-based films have lower adhesion forces to surfaces, due to the stronger hydration of these brushes in the high-ionic-strength media.[163]

4 | CONCLUSIONS AND OUTLOOK

AFM has become an indispensable tool for both fundamental polymer physics and functional applications research due to its unique capacity for multifunctional characterization and imaging. AFM imaging has highlighted the rich complexity and heterogeneity of polymers at the nanoscale: It has helped elucidate mechanisms of polymer ordering, phase separation, and crystallization, as well as correlated nanoscale structures to

functionality in relation to membranes and electronics applications. In this Perspective, we have highlighted some of the current and forefront polymer issues using AFM to study the function and structure of polymer films. Ongoing developments in AFM technology, including high-speed, high-resolution, and multiparametric imaging, with improved environmental controls for in situ temperature and solution imaging, continue to provide insight into polymer dynamics and interactions under real world conditions. As new and increasingly complex polymer materials are continually designed, we may anticipate that, in the future, the unique capabilities of AFM will help resolve outstanding issues and guide the formulation of new questions at the frontier of polymer science.

ORCID

Julia G. Murphy ⓘ https://orcid.org/0000-0001-6334-559X
Jonathan G. Raybin ⓘ https://orcid.org/0000-0001-9040-4241
Steven J. Sibener ⓘ https://orcid.org/0000-0002-5298-5484

REFERENCES AND NOTES

[1] G. J. Vancso, H. Schönherr, *Scanning Force Microscopy of Polymers*, Springer-Verlag, Berlin Heidelberg **2010**.

[2] M. E. McConney, S. Singamaneni, V. V. Tsukruk, *Polym. Rev.* **2010**, *50*, 235.

[3] D. Wang, T. P. Russell, *Macromolecules* **2018**, *22*, 3.

[4] G. H. Michler, *Appl. Spectrosc. Rev.* **1993**, *28*, 327.

[5] B. Chu, B. S. Hsiao, *Chem. Rev.* **2001**, *101*, 1727.

[6] A. Hexemer, P. Müller-Buschbaum, *IUCrJ* **2015**, *2*, 106.

[7] J. S. Trent, J. I. Scheinbeim, P. R. Couchman, *Macromolecules* **1983**, *16*, 589.

[8] C. G. Bischak, C. L. Hetherington, Z. Wang, J. T. Precht, D. M. Kaz, D. G. Schlom, N. S. Ginsberg, *Nano Lett.* **2015**, *15*, 3383.

[9] T. Albrecht, G. Strobl, *Macromolecules* **1996**, *29*, 783.

[10] D. Posselt, J. Zhang, D.-M. Smilgies, A. V. Berezkin, I. I. Potemkin, C. M. Papadakis, *Prog. Polym. Sci.* **2017**, *66*, 80.

[11] G. Binnig, C. F. Quate, C. Gerber, *Phys. Rev. Lett.* **1986**, *56*, 930.

[12] B. Drake, C. B. Prater, A. L. Weisenhorn, S. A. Gould, T. R. Albrecht, C. F. Quate, D. S. Cannell, H. G. Hansma, P. K. Hansma, *Science* **1989**, *243*, 1586.

[13] T. Ando, N. Kodera, E. Takai, D. Maruyama, K. Saito, A. Toda, *Proc. Natl. Acad. Sci. U. S. A.* **2001**, *98*, 12468.

[14] R. Garcia, R. Perez, *Surf. Sci. Rep.* **2002**, *47*, 197.

[15] R. Garcia, E. T. Herruzo, *Nat. Nanotechnol.* **2012**, *7*, 217.

[16] Y. F. Dufrêne, T. Ando, R. Garcia, D. Alsteens, D. Martinez-Martin, A. Engel, C. Gerber, D. J. Müller, *Nat. Nanotechnol.* **2017**, *12*, 295.

[17] R. Garcia, *Chem. Soc. Rev.* **2020**, *49*, 5850.

[18] H. G. Hansma, J. H. Hoh, *Annu. Rev. Biophys.* **1994**, *23*, 115.

[19] H. G. Hansma, L. I. Pietrasanta, I. D. Auerbach, C. Sorenson, R. Golan, P. A. Holden, *J. Biomater. Sci. Polym. Ed.* **2000**, *11*, 675.

[20] S. Liu, Y. Wang, *Scanning* **2010**, *32*, 61.

[21] F. J. Giessibl, *Jpn. J. Appl. Phys.* **1994**, *33*, 3726.

[22] L. Chen, X. Gu, M. J. Fasolka, J. W. Martin, T. Nguyen, *Langmuir* **2009**, *25*, 3494.

[23] C. Marcuello, L. Foulon, B. Chabbert, V. Aguié-Béghin, M. Molinari, *Int. J. Biol. Macromol.* **2020**, *147*, 1064.

[24] M. J. Fasolka, A. M. Mayes, S. N. Magonov, *Ultramicroscopy* **2001**, *90*, 21.

[25] Y. Kikkawa, H. Abe, M. Fujita, T. Iwata, Y. Inoue, Y. Doi, *Macromol. Chem. Phys.* **2003**, *204*, 1822.

[26] J.-J. Zhou, J.-G. Liu, S.-K. Yan, J.-Y. Dong, L. Li, C.-M. Chan, J. M. Schultz, *Polymer* **2005**, *46*, 4077.

[27] P. K. Hansma, J. P. Cleveland, M. Radmacher, D. A. Walters, P. E. Hillner, M. Bezanilla, M. Fritz, D. Vie, H. G. Hansma, C. B. Prater, J. Massie, L. Fukunaga, J. Gurley, V. B. Elings, *Appl. Phys. Lett.* **1994**, *64*, 1738.

[28] J. P. Cleveland, B. Anczykowski, A. E. Schmid, V. B. Elings, *Appl. Phys. Lett.* **1998**, *72*, 2613.

[29] D. Raghavan, X. Gu, T. Nguyen, M. VanLandingham, A. Karim, *Macromolecules* **2000**, *33*, 2573.

[30] R. Proksch, D. G. Yablon, *Appl. Phys. Lett.* **2012**, *100*, 73106.

[31] R. Proksch, M. Kocun, D. Hurley, M. Viani, A. Labuda, W. Meinhold, J. Bemis, *J. Appl. Phys.* **2016**, *119*, 134901.

[32] R. Proksch, *Appl. Phys. Lett.* **2006**, *89*, 113121.

[33] S. Santos, C.-Y. Lai, T. Olukan, M. Chiesa, *Nanoscale* **2017**, *9*, 5038.

[34] G. Benstetter, R. Biberger, D. Liu, *Thin Solid Films* **2009**, *517*, 5100.

[35] W. Melitz, J. Shen, A. C. Kummel, S. Lee, *Surf. Sci. Rep.* **2011**, *66*, 1.

[36] J. Jahng, D. A. Fishman, S. Park, D. B. Nowak, W. A. Morrison, H. K. Wickramasinghe, E. O. Potma, *Acc. Chem. Res.* **2015**, *48*, 2671.

[37] A. Dazzi, C. B. Prater, *Chem. Rev.* **2017**, *117*, 5146.

[38] C. L. Bentley, J. Edmondson, G. N. Meloni, D. Perry, V. Shkirskiy, P. R. Unwin, *Anal. Chem.* **2019**, *91*, 84.

[39] T. Ando, T. Uchihashi, T. Fukuma, *Prog. Surf. Sci.* **2008**, *83*, 337.

[40] T. Ando, *Nanotechnology* **2012**, *23*, 62001.

[41] T. Ando, T. Uchihashi, N. Kodera, *Annu. Rev. Biophys.* **2013**, *42*, 393.

[42] T. Ando, *Curr. Opin. Struct. Biol.* **2014**, *28*, 63.

[43] P. K. Hansma, G. Schitter, G. E. Fantner, C. Prater, *Science* **2006**, *314*, 601.

[44] D. A. Walters, J. P. Cleveland, N. H. Thomson, P. K. Hansma, M. A. Wendman, G. Gurley, V. Elings, *Rev. Sci. Instrum.* **1996**, *67*, 3583.

[45] G. E. Fantner, G. Schitter, J. H. Kindt, T. Ivanov, K. Ivanova, R. Patel, N. Holten-Andersen, J. Adams, P. J. Thurner, I. W. Rangelow, P. K. Hansma, *Ultramicroscopy* **2006**, *106*, 881.

[46] T. Sulchek, R. Hsieh, J. D. Adams, S. C. Minne, C. F. Quate, D. M. Adderton, *Rev. Sci. Instrum.* **2000**, *71*, 2097.

[47] A. D. L. Humphris, M. J. Miles, J. K. Hobbs, *Appl. Phys. Lett.* **2005**, *86*, 034106.

[48] T. E. Schäffer, J. P. Cleveland, F. Ohnesorge, D. A. Walters, P. K. Hansma, *J. Appl. Phys.* **1996**, *80*, 3622.

[49] S. Tien, Q. Zou, S. Devasia, *IEEE Trans. Contr. Syst. Technol.* **2005**, *13*, 921.

[50] A. Labuda, K. Kobayashi, D. Kiracofe, K. Suzuki, P. H. Grütter, H. Yamada, *AIP Adv.* **2011**, *1*, 022136.

[51] A. Labuda, K. Kobayashi, Y. Miyahara, P. Grütter, *Rev. Sci. Instrum.* **2012**, *83*, 053703.

[52] A. Labuda, S. Hohlbauch, M. Kocun, F. T. Limpoco, N. Kirchhofer, B. Ohler, D. Hurley, *Microsc. Today* **2018**, *26*, 12.

[53] N. Kodera, D. Yamamoto, R. Ishikawa, T. Ando, *Nature* **2010**, *468*, 72.

[54] T. Fukui, T. Uchihashi, N. Sasaki, H. Watanabe, M. Takeuchi, K. Sugiyasu, *Angew. Chem., Int. Ed.* **2018**, *57*, 15465.

[55] K. Ushimaru, S. Mizuno, A. Honya, H. Abe, T. Tsuge, *ACS Omega* **2017**, *2*, 181.

[56] J. Raybin, J. Ren, X. Chen, R. Gronheid, P. F. Nealey, S. J. Sibener, *Nano Lett.* **2017**, *17*, 7717.

[57] T. Brouns, H. De Keersmaecker, S. F. Konrad, N. Kodera, T. Ando, J. Lipfert, S. De Feyter, W. Vanderlinden, *ACS Nano* **2018**, *12*, 11907.

[58] Y. Zhang, M. Hashemi, Z. Lv, B. Williams, K. I. Popov, N. V. Dokholyan, Y. L. Lyubchenko, *J. Chem. Phys.* **2018**, *148*, 123322.

[59] J. A. Kretzmann, C. W. Evans, L. Feng, N. B. Lawler, M. Norret, M. J. Higgins, K. S. Iyer, *Langmuir* **2020**, *36*, 9074.

[60] M. Soliman, Y. Ding, L. Tetard, *J. Phys.: Condens. Matter* **2017**, *29*, 173001.

[61] E.-C. Spitzner, C. Riesch, R. Magerle, *ACS Nano* **2011**, *5*, 315.

[62] D. Ebeling, B. Eslami, S. D. J. Solares, *ACS Nano* **2013**, *7*, 10387.

[63] L. Mester, A. A. Govyadinov, S. Chen, M. Goikoetxea, R. Hillenbrand, *Nat. Commun.* **2020**, *11*, 3359.

[64] B. Cappella, G. Dietler, *Surf. Sci. Rep.* **1999**, *34*, 1.

[65] H.-J. Butt, B. Cappella, M. Kappl, *Surf. Sci. Rep.* **2005**, *59*, 1.

[66] A. A. Tseng, *Small* **2011**, *7*, 3409.

[67] R. Garcia, A. W. Knoll, E. Riedo, *Nat. Nanotech* **2014**, *9*, 577.

[68] Y. Krivoshapkina, M. Kaestner, I. W. Rangelow, in *Frontiers of Nanoscience* (Eds: A. Robinson, R. Lawson), Amsterdam: Elsevier, **2016**, p. 497.

[69] M. Hirtz, M. K. Brinks, S. Miele, A. Studer, H. Fuchs, L. Chi, *Small* **2009**, *5*, 919.

[70] J. Duvigneau, H. Schönherr, G. J. Vancso, *ACS Nano* **2010**, *4*, 6932.

[71] S. T. Howell, A. Grushina, F. Holzner, J. Brugger, *Microsyst. Nanoeng.* **2020**, *6*, 1.

[72] G. Liu, S. H. Petrosko, Z. Zheng, C. A. Mirkin, *Chem. Rev.* **2020**, *120*, 6009.

[73] P. Vettiger, G. Cross, M. Despont, U. Drechsler, U. Durig, B. Gotsmann, W. Haberle, M. A. Lantz, H. E. Rothuizen, R. Stutz, G. K. Binnig, *IEEE Trans. Nanotechnol.* **2002**, *1*, 39.

[74] M. Muthukumar, in *Progress in Understanding of Polymer Crystallization* (Eds: G. Reiter, G. R. Strobl), Springer, Berlin, Heidelberg **2007**.

[75] X. Tang, W. Chen, L. Li, *Macromolecules* **2019**, *17*, 3575.

[76] J. K. Hobbs, O. E. Farrance, L. Kailas, *Polymer* **2009**, *50*, 4281.

[77] T. P. Lodge, *Macromolecules* **2017**, *50*, 9525.

[78] J. I. Lauritzen, J. D. Hoffman, *J. Res. Natl. Bur. Stand. A Phys. Chem* **1960**, *64A*, 73.

[79] T. Hugel, G. Strobl, R. Thomann, *Acta Polym.* **1999**, *50*, 214.

[80] L. Li, C.-M. Chan, K. L. Yeung, J.-X. Li, K.-M. Ng, Y. Lei, *Macromolecules* **2001**, *34*, 316.

[81] G. Strobl, *Eur. Phys. J. E: Soft Matter Biol. Phys.* **2000**, *3*, 165.

[82] J. Kumaki, T. Kawauchi, E. Yashima, *J. Am. Chem. Soc.* **2005**, *127*, 5788.

[83] Y. Ono, J. Kumaki, *Macromolecules* **2018**, *51*, 7629.

[84] V. V. Korolkov, A. Summerfield, A. Murphy, D. B. Amabilino, K. Watanabe, T. Taniguchi, P. H. Beton, *Nat. Commun.* **2019**, *10*, 1537.

[85] D. E. Acevedo-Cartagena, J. Zhu, M. Kocun, S. S. Nonnenmann, R. C. Hayward, *Macromolecules* **2019**, *52*, 7756.

[86] X. Lyu, Y. Song, W. Feng, W. Zhang, *ACS Macro Lett.* **2018**, *7*, 762.

[87] Y. Song, Z. Ma, P. Yang, X. Zhang, X. Lyu, K. Jiang, W. Zhang, *Macromolecules* **2019**, *52*, 1327.

[88] K. Liu, Y. Song, W. Feng, N. Liu, W. Zhang, X. Zhang, *J. Am. Chem. Soc.* **2011**, *133*, 3226.

[89] C. M. Bates, M. J. Maher, D. W. Janes, C. J. Ellison, C. G. Willson, *Macromolecules* **2014**, *47*, 2.

[90] R. Ruiz, H. Kang, F. A. Detcheverry, E. Dobisz, D. S. Kercher, T. R. Albrecht, J. J. de Pablo, P. F. Nealey, *Science* **2008**, *321*, 936.

[91] F. Bates, G. Fredrickson, *Annu. Rev. Phys. Chem.* **1990**, *41*, 525.

[92] S. B. Darling, *Prog. Polym. Sci.* **2007**, *32*, 1152.

[93] D. Sundrani, S. B. Darling, S. J. Sibener, *Langmuir* **2004**, *20*, 5091.

[94] S. Ouk Kim, H. H. Solak, M. P. Stoykovich, N. J. Ferrier, J. J. de Pablo, P. F. Nealey, *Nature* **2003**, *424*, 411.

[95] Q. Tong, Q. Zheng, S. J. Sibener, *Macromolecules* **2014**, *47*, 4236.

[96] M. A. van Dijk, R. van den Berg, *Macromolecules* **1995**, *28*, 6773.

[97] A. Knoll, A. Horvat, K. S. Lyakhova, G. Krausch, G. J. A. Sevink, A. V. Zvelindovsky, R. Magerle, *Phys. Rev. Lett.* **2002**, *89*, 035501.

[98] A. Knoll, R. Magerle, G. Krausch, *Macromolecules* **2001**, *34*, 4159.

[99] Q. Zhang, O. K. C. Tsui, B. Du, F. Zhang, T. Tang, T. He, *Macromolecules* **2000**, *33*, 9561.

[100] K. W. Gotrik, A. F. Hannon, J. G. Son, B. Keller, A. Alexander-Katz, C. A. Ross, *ACS Nano* **2012**, *6*, 8052.

[101] J. Hayat, I. Mitra, Y. Qiao, G. E. Stein, C. Tang, *Eur. Polym. J.* **2015**, *71*, 476.

[102] H. Zhang, B. Wang, G. Wang, C. Shen, J. Chen, G. Reiter, B. Zhang, *Macromolecules* **2020**, *53*, 9631.

[103] K. Takano, T. Nyu, T. Maekawa, T. Seki, R. Nakatani, T. Komamura, T. Hayakawa, T. Hayashi, *RSC Adv.* **2020**, *10*, 70.

[104] A. Modi, S. M. Bhaway, B. D. Vogt, J. F. Douglas, A. Al-Enizi, A. Elzatahry, A. Sharma, A. Karim, *ACS Appl. Mater. Interfaces* **2015**, *7*, 21639.

[105] M. Longanecker, A. Modi, A. Dobrynin, S. Kim, G. Yuan, R. Jones, S. Satija, J. Bang, A. Karim, *Macromolecules* **2016**, *49*, 8563.

[106] C. Harrison, D. H. Adamson, Z. Cheng, J. M. Sebastian, S. Sethuraman, D. A. Huse, R. A. Register, P. M. Chaikin, *Science* **2000**, *290*, 1558.

[107] J. Hahm, W. A. Lopes, H. M. Jaeger, S. J. Sibener, *J. Chem. Phys.* **1998**, *109*, 10111.

[108] J. Hahm, S. J. Sibener, *J. Chem. Phys.* **2001**, *114*, 4730.

[109] Q. Tong, S. J. Sibener, *Macromolecules* **2013**, *46*, 8538.

[110] H. J. Ryu, Q. Tong, S. J. Sibener, *J. Phys. Chem. Lett.* **2013**, *4*, 2890.

[111] F. Stehlin, F. Diot, A. Gwiazda, A. Dirani, M. Salaun, M. Zelsmann, O. Soppera, *Langmuir* **2013**, *29*, 12796.

[112] N. A. Yufa, J. Li, S. J. Sibener, *Polymer* **2009**, *50*, 2630.

[113] A. Chandra, R. Nakatani, T. Uchiyama, Y. Seino, H. Sato, Y. Kasahara, T. Azuma, T. Hayakawa, *Adv. Mater. Interfaces* **2019**, *6*, 1801401.

[114] C. T. Bezik, J. J. de Pablo, *Macromolecules* **2020**, *53*, 10446.

[115] J. G. Raybin, J. G. Murphy, M. Dolejsi, S. J. Sibener, *ACS Nano* **2019**, *13*, 11741.

[116] B. Pollard, E. A. Muller, K. Hinrichs, M. B. Raschke, *Nat. Commun.* **2014**, *5*, 3587.

[117] D. Nowak, W. Morrison, H. K. Wickramasinghe, J. Jahng, E. Potma, L. Wan, R. Ruiz, T. R. Albrecht, K. Schmidt, J. Frommer, D. P. Sanders, S. Park, *Sci. Adv.* **2016**, *2*, e1501571.

[118] L. Wang, H. Wang, M. Wagner, Y. Yan, D. S. Jakob, X. G. Xu, *Sci. Adv.* **2017**, *3*, e1700255.

[119] L. S. C. Pingree, O. G. Reid, D. S. Ginger, *Adv. Mater.* **2009**, *21*, 19.

[120] M. Osaka, D. Mori, H. Benten, H. Ogawa, H. Ohkita, S. Ito, *ACS Appl. Mater. Interfaces* **2017**, *9*, 15615.

[121] N. Spampinato, G. Pecastaings, M. Maglione, G. Hadziioannou, E. Pavlopoulou, *Colloid Polym. Sci.* **2021**, *299*, 551.

[122] O. G. Reid, K. Munechika, D. S. Ginger, *Nano Lett.* **2008**, *8*, 1602.

[123] E. Daviddi, Z. Chen, B. Beam Massani, J. Lee, C. L. Bentley, P. R. Unwin, E. L. Ratcliff, *ACS Nano* **2019**, *13*, 13271.

[124] M. Osaka, H. Benten, H. Ohkita, S. Ito, *Macromolecules* **2017**, *50*, 1618.

[125] C. Groves, O. G. Reid, D. S. Ginger, *Acc. Chem. Res.* **2010**, *43*, 612.

[126] D. C. Coffey, O. G. Reid, D. B. Rodovsky, G. P. Bartholomew, D. S. Ginger, *Nano Lett.* **2007**, *7*, 738.

[127] J. L. Luria, N. Hoepker, R. Bruce, A. R. Jacobs, C. Groves, J. A. Marohn, *ACS Nano* **2012**, *6*, 9392.

[128] S. Pont, F. Foglia, A. M. Higgins, J. R. Durrant, J. T. Cabral, *Adv. Funct. Mater.* **2018**, *28*, 1802520.

[129] V. Abetz, *Macromol. Rapid Commun.* **2015**, *36*, 10.

[130] A. Lee, J. W. Elam, S. B. Darling, *Environ. Sci: Water Res. Technol.* **2016**, *2*, 17.

[131] S. P. Nunes, *Macromolecules* **2016**, *49*, 2905.

[132] H.-C. Yang, Y. Xie, J. Hou, A. K. Cheetham, V. Chen, S. B. Darling, *Adv. Mater.* **2018**, *30*, 1801495.

[133] D. J. Lyman, *ASAIO J.* **1963**, *9*, 92.

[134] D. J. Lyman, B. H. Loo, R. W. Crawford, *Biochemistry* **1964**, *3*, 985.

[135] S. P. Nunes, M. L. Sforça, K.-V. Peinemann, *J. Membr. Sci.* **1995**, *106*, 49.

[136] S. Y. Yang, I. Ryu, H. Y. Kim, J. K. Kim, S. K. Jang, T. P. Russell, *Adv. Mater.* **2006**, *18*, 709.

[137] K.-V. Peinemann, V. Abetz, P. F. W. Simon, *Nat. Mater.* **2007**, *6*, 992.

[138] Z. Wang, X. Yao, Y. Wang, *J. Mater. Chem.* **2012**, *22*, 20542.

[139] R. Z. Waldman, H.-C. Yang, D. J. Mandia, P. F. Nealey, J. W. Elam, S. B. Darling, *Adv. Mater. Interfaces* **2018**, *5*, 1800658.

[140] R. Z. Waldman, N. Jeon, D. J. Mandia, O. Heinonen, S. B. Darling, A. B. F. Martinson, *Chem. Mater.* **2019**, *31*, 5274.

[141] W. R. Bowen, T. A. Doneva, *Surf. Interface Anal.* **2000**, *29*, 544.

[142] A. M. ElHadidy, S. Peldszus, M. I. Van Dyke, *J. Membr. Sci.* **2013**, *429*, 373.

[143] D. Y. Khanukaeva, A. N. Filippov, A. V. Bildyukevich, *Pet. Chem.* **2014**, *54*, 498.

[144] K. Boussu, B. Van der Bruggen, A. Volodin, J. Snauwaert, C. Van Haesendonck, C. Vandecasteele, *J. Colloid Interface Sci.* **2005**, *286*, 632.

[145] Y. Wyart, R. Tamime, L. Siozade, I. Baudin, K. Glucina, C. Deumié, P. Moulin, *J. Membr. Sci.* **2014**, *472*, 241.

[146] A. J. Bard, F. R. F. Fan, J. Kwak, O. Lev, *Anal. Chem.* **1989**, *61*, 132.

[147] J. V. Macpherson, P. R. Unwin, *Anal. Chem.* **2000**, *72*, 276.

[148] S. Amemiya, A. J. Bard, F.-R. F. Fan, M. V. Mirkin, P. R. Unwin, *Annu. Rev. Anal. Chem.* **2008**, *1*, 95.

[149] A. Davoodi, A. Farzadi, J. Pan, C. Leygraf, Y. Zhu, *J. Electrochem. Soc.* **2008**, *155*, C474.

[150] X. Shi, W. Qing, T. Marhaba, W. Zhang, *Electrochim. Acta* **2020**, *332*, 135472.

[151] E. R. Scott, H. S. White, *Anal. Chem.* **1993**, *65*, 1537.

[152] O. D. Uitto, H. S. White, *Anal. Chem.* **2002**, *74*, 4577.

[153] C. E. Gardner, P. R. Unwin, J. V. Macpherson, *Electrochem. Commun.* **2005**, *7*, 612.

[154] P. J. Flory, *J. Chem. Phys.* **1941**, *9*, 660.

[155] M. L. Huggins, *J. Chem. Phys.* **1941**, *9*, 440.

[156] Y. Lai, Y. Hu, *Soft Matter* **2018**, *14*, 2619.

[157] J. G. Raybin, S. J. Sibener, *Macromolecules* **2019**, *52*, 5985.

[158] D. Messmer, O. Bertran, R. Kissner, C. Alemán, A. D. Schlüter, *Chem. Sci.* **2019**, *10*, 6125.

[159] A. D. Schlüter, A. Halperin, M. Kröger, D. Vlassopoulos, G. Wegner, B. Zhang, *ACS Macro Lett.* **2014**, *3*, 991.

[160] K. Jalili, F. Abbasi, L. Behboodpour, *J. Mech. Behav. Biomed. Mater.* **2019**, *93*, 118.

[161] M. R. Hibbs, B. A. Hernandez-Sanchez, J. Daniels, S. J. Stafslien, *Biofouling* **2015**, *31*, 613.

[162] Y. Higaki, J. Nishida, A. Takenaka, R. Yoshimatsu, M. Kobayashi, A. Takahara, *Polym. J.* **2015**, *47*, 811.

[163] S. Guo, R. Quintana, M. Cirelli, Z. S. D. Toa, V. Arjunan Vasantha, E. S. Kooij, D. Jańczewski, G. J. Vancso, *Langmuir* **2019**, *35*, 8085.

AUTHOR BIOGRAPHIES

Julia G. Murphy is currently a doctoral candidate at the University of Chicago under the supervision of Prof. Steven Sibener. Her research focuses on understanding the self-organizing and surface dynamics of polymer thin films with in situ AFM.

Jonathan G. Raybin received his Ph.D. in Chemistry from the University of Chicago under the supervision of Prof. Steven Sibener investigating BCP dynamics with high-speed AFM. He is currently at the University of California, Berkeley working in the lab of Prof. Naomi Ginsberg, where he is studying colloidal self assembly.

Steven J. Sibener is the Carl William Eisendrath Distinguished Service Professor in the Department of Chemistry and The James Franck Institute of the University of Chicago. He received his doctorate at Berkeley, and was a postdoctoral researcher at Bell Laboratories. He has research interests that focus on the interfacial behavior of materials including polymers, semiconductors, metals, superconductors, water, and ice. Such systems are examined using scanning probe methods, gas-surface neutral particle scattering, and MD simulations.